Growth of Si nanorods in honeycomb and hexagonal-closed-packed arrays using glancing angle deposition

Christian Patzig,[1,a)] Bernd Rauschenbach,[1] Bodo Fuhrmann,[2] and Hartmut S. Leipner[2]
[1]*Leibniz-Institut für Oberflächenmodifizierung e.V., Permoserstraße 15, 04318 Leipzig, Germany*
[2]*Interdisziplinäres Zentrum für Materialwissenschaften, Martin-Luther-Universität Halle, Heinrich-Damerow-Straße 4, 06120 Halle, Germany*

(Received 16 July 2007; accepted 23 November 2007; published online 29 January 2008)

Regular arrays of Si nanorods with a circular cross section in hexagonal-closed-packed and triangular cross section in honeycomblike arrangements were grown using glancing angle deposition on Si(100) and fused silica substrates that were patterned with Au dots using self-assembled mono- and double layers of polystyrene nanospheres as an evaporation mask. The Au dots were used as an etching mask for the underlying silica substrates in a reactive ion beam etching process, which greatly enhanced the height of the seeding spaces for the subsequent glancing angle deposition. An elongated shadowing length l of the prepatterned nucleation sites and less growth of Si structures between the surface mounds could be achieved this way. Differences in form, height, and diameter of the Si nanorods grown on either hcp or honeycomb arrays are explained by purely geometrical arguments. Different seed heights and interseed distances are found to be the main reasons for the strong distinctions between the grown nanorod arrays. © *2008 American Institute of Physics*. [DOI: 10.1063/1.2836962]

I. INTRODUCTION

The glancing angle deposition[1] (GLAD) process is a physical vapor deposition process in which the incoming particle flux reaches the substrate under a highly oblique angle β as measured to the substrate normal. Due to this deposition regime, atomic shadowing of neighbored islands and clusters on the substrate leads to the growth of highly porous thin films, consisting of needlelike structures that are slanted in the direction of the incoming particle flux. In combination with a suitable substrate rotation, unique structures such as nanopillars, nanospirals, and nanochevrons can be grown.[2,3] Potential applications span a wide range, including photonic crystals,[4] polarizing filters,[5] humidity sensors,[6] thermal barrier coatings,[7] and even supports for enzyme immobilization.[8] However, as a result of the stochastic nucleation process on nonpatterned substrates, the growth of nanostructures via the GLAD on flat substrates usually generates randomly distributed nonuniform structures that broaden with increasing height[9] and show a competitive growth mode of adjacent structures that can lead to the extinction of some of the structures. In order to grow well-aligned, regularly arranged nanostructures with defined periodicity and constant structure diameter, patterned substrates have to be used. In this case, the patterned mounds of distinct height and diameter serve as nucleation sites for the incoming particles. Usual patterning methods include electron beam lithography[3,10] and nanosphere lithography (NSL), where in the latter either the nanospheres themselves serve as seeding spaces,[2,11,12] or the hexagonal-closed-packed (hcp) arranged nanosphere monolayers are used as an evaporation mask for the subsequent patterning of the substrates with an evaporant passing through the spaces between the spheres, thus forming a honeycomb pattern on the substrate, followed by the removal of the nanosphere layer.[13]

In this work, the NSL technique with usage of the nanospheres as an evaporation mask was extended in so far that not only monolayers but also double layers of nanospheres were used as Au evaporation masks. Thus, not only honeycomb but also hcp Au arrays as seeding spaces for the incoming Si particle flux could be created. Additionally, for some samples the Au dots were used as an etching mask in a reactive ion beam etching process themselves, making use of the different etching rates of Au and the underlying silica substrate. The aspect ratio of height and interseed distance could be increased this way, leading to less perturbing growth between the seeds.

Si nanorod structures grown on prepatterned substrates with different seeding space heights and different interseed distances are compared regarding diameter and shape. It is shown that the interseed spacing rules both diameter and form of the Si nanorods and that the effects of geometric shadowing control the growth of the structures, whereas surface diffusion is negligible for room temperature deposition.

II. EXPERIMENTAL

Figure 1 illustrates the patterning of the substrates, which was performed as described in an earlier work.[14] Si(100) substrates were patterned with monolayers (ML) and double layers (DL) of nanospheres of diameter $D=419$ nm and $D=508$ nm and fused silica substrates were patterned with nanospheres of $D=508$ nm. After evaporating Au layers of nominal thicknesses of 5 and 35 nm onto those substrates, the nanospheres were removed, leaving honeycomblike arranged Au dots with nearest-neighbor distances d of $d\approx 240$ nm ($D=419$ nm) and $d\approx 290$ nm ($D=508$ nm) in

a)Electronic mail: christian.patzig@iom-leipzig.de.

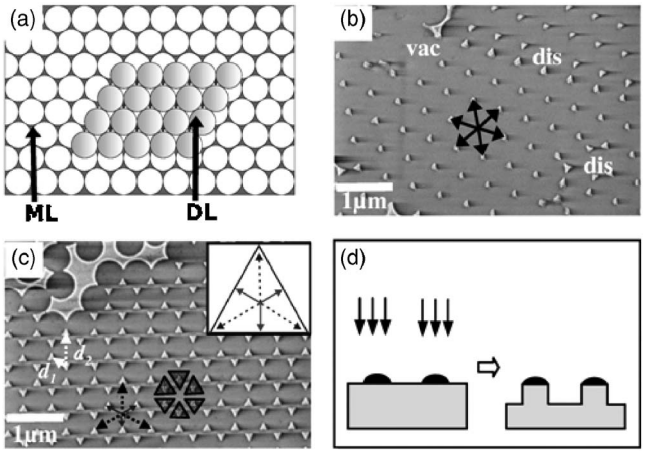

FIG. 1. (a) Sketch of a monolayer and a double layer of hcp nanospheres to underline how the hcp array (b) and the honeycomb array (c) of Au dots are created by evaporating through the spaces between the spheres. (d) Principle of the structure transformation from the Au dots into the substrate.

the ML case, or, in the DL case, leaving hcp arranged Au dots with $d \approx 420$ nm ($D=419$ nm) and $d \approx 510$ nm ($D=508$ nm). Defects like dislocations (dis) and vacancies (vac) are shown in Fig. 1(b). As can be seen, the resulting seeding spaces of the honeycomblike ML pattern are quasi-triangular, whereas the seeding spaces of the hcp Au dots of the DL evaporation mask are conelike.

Before performing the GLAD experiments, the patterned silica substrates with Au dots of $h=35$ nm height were etched in a reactive ion beam etching process, using a mixture of CHF_3 and O_2 (97.5%/2.5%) as the etching gas. The different etching rates of Au and fused silica resulted in a structure transfer from the Au dot pattern in the substrate itself, as illustrated in Fig. 1(d). Etching times of 3 and 5 min yielded an enhancement of the height of the seeding space from $h=35$ nm to $h=90$ nm or to $h=150$ nm, respectively.

The Si nanorods were grown using the GLAD by ion beam sputtering with an experimental setup as described elsewhere[3,10,15,16] in a high vacuum chamber with a base pressure of approximately 1.0×10^{-8} mbar. A sintered polycrystalline Si disk used as a target is sputtered by an Ar^+-ion beam extracted out of an inductively coupled, high-frequency (13.56 MHz) ion source with a focusing triple grid system of 40 mm in diameter. An argon flux of $f_{Ar}=5.0$ sccm resulted in a working pressure of 9.0×10^{-5} mbar. The substrates were attached to a substrate holder with a continuously variable substrate tilt β and a computer-controlled step motor was used to continuously rotate the substrate around the substrate normal with an rotational speed $\omega=0.2$ rev/min. The ion source-target distance measured 15 cm and the target-substrate distance was 12 cm. The ion energy was set to 1100 eV and the ion beam reached the target under an angle $\phi_{Target}=65°$ to the target normal. The angle β of the incoming Si vapor flux was set to $\beta=83°$. A slit aperture between the target and the substrate was used in order to minimize the angular divergence $\Delta\beta$ of the Si particles reaching the substrate. This experimental setup led to a vertical growth rate of approximately 3.7 nm/min for the Si nanorods. All experiments were performed at room temperature.

The nanorods on the $D=419$ nm honeycomb and hcp patterns with heights of the Au dots of $h=3$ nm and $h=35$ nm were grown with a deposition time $t=135$ min, thus leading to Si nanorods with a nominal height of $t=500$ nm, whereas the nanorods on the $D=508$ nm patterns with $h=35$ nm, $h=95$ nm, and $h=150$ nm were grown with a deposition time of $t=185$ min, yielding Si nanorods with nominal heights of $t=685$ nm. After growth, the samples were cleaved and studied using scanning electron microscopy (SEM) at 2.5 kV acceleration voltage. The analysis of the micrographs was done using the commercially available Scanning Probe Image Processor[17] version 3.2.6.0 (SPIP), using the fast Fourier transformation and grain detection modules.

III. RESULTS AND DISCUSSION

Figure 2(a) shows a top view SEM image of Si nanorods

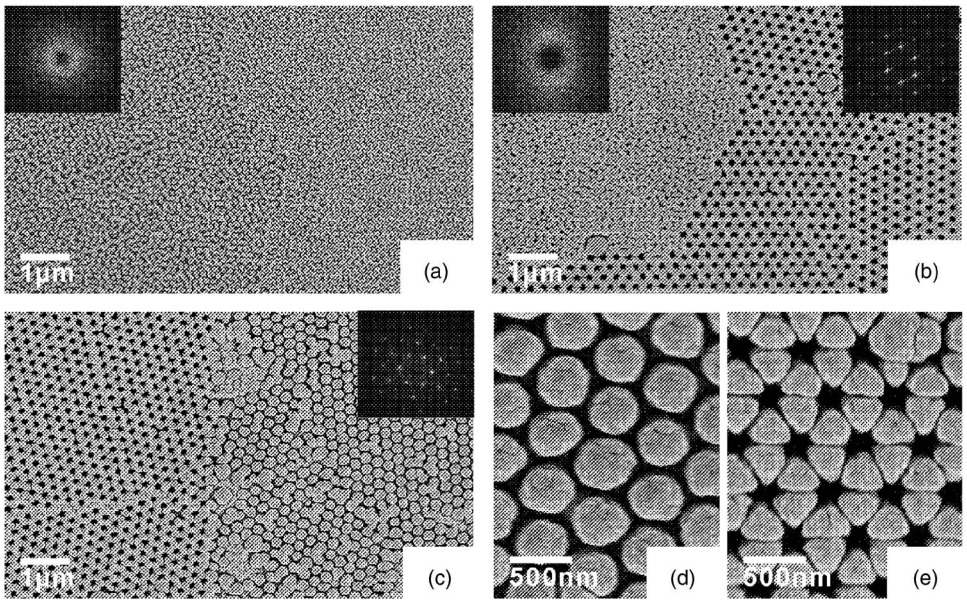

FIG. 2. Top-view SEM pictures of Si nanorods. (a) Transition region between rods grown on honeycomblike arranged Au dots (left part) and rods grown on flat substrate (right part). (b) Transition region between rods grown on flat substrate (left part) and rods grown on honeycomb patterns of Au dots (right part). (c) Transition region between rods grown on a honeycomb pattern (left part) and rods grown on a hcp pattern (right part). (d) and (e) show magnifications for the hcp pattern and the honeycomb pattern of (c). Insets of (a)–(c): Fourier images calculated from top-view high resolution SEM micrographs for the respective type of seed pattern.

grown on seeding spaces with $h=5$ nm adjacent to nanorods grown on an unpatterned part of the same substrate for a nanosphere diameter of $D=419$ nm. As can be seen in this figure, the honeycomb arrangement of the seed pattern is not adopted by the nanostructured Si layer. Although some part of the Si flux is captured by the Au hillocks, leading to broader nanorods as compared to the ones grown on the flat substrate, a significant portion of the Si vapor flux is still capable to reach the substrate between the seeds, thus leading to nonignorable growth of nanorods on the substrate rather than on the seeding spaces. The reason for this interseed growth is the insufficient height of the Au dots. The shadowing length l [see Fig. 4(d)], which is the distance on the substrate an obstacle of height h is capable to shadow, is a function of the angle β of the incoming particle flux: $l=h/\tan(90°-\beta)$. Hence, for $\beta=83°$ and $h=5$ nm, we get $l\approx 40$ nm. For $D=419$ nm, the nearest-neighbor distance of the honeycomblike ML seeding spaces is $d\approx 240$ nm. Therefore, only approximately 1/6 of d is shadowed by the Au dots and significant growth between the seeds occurs.

Increasing the height of the seeding spaces from $h=5$ nm to $h=35$ nm increases the shadowing length l from $l\approx 40$ nm to $l\approx 280$ nm and results in a drastic change of the geometrical shadowing conditions, as can be seen in Figs. 2(b) and 2(c) for the case of $D=508$ nm. Now most of the particle flux that impinges on the substrate gets caught by the seeding spaces, and, as a result, the growing film consists of nanorods that perfectly adopt the periodicity of the seed pattern. The insets in Figs. 2(a)–2(c) show two-dimensional-Fourier images calculated from high resolution top-view SEM micrographs. As is observable in Fig. 2(a), the Fourier image of the nanorods grown on Au dots with $h=5$ nm resembles a bright ring, indicating a preferred inter-rod distance,[18] but showing no periodic arrangement of the rods. In fact, it is comparable to the Fourier image of nanorods grown on a flat substrate, as can be seen in the left inset in Fig. 2(b). On the contrary, the Fourier images of the nanorods grown on the ML honeycomb pattern and on the DL hcp pattern with seed heights of $h=35$ nm perfectly display the hexagonal arrangement of the Si structures on the seeding spaces.

Figures 2(d) and 2(e) reveal that form and diameter of the Si nanorods grown on hcp and honeycomblike arranged seeds of equal height h and equal nanosphere diameter D differ strongly. Rods grown on hcp seeds are cylindrical, having a circular cross section, whereas the Si nanostructures grown on honeycomblike arranged seeds have a triangular cross section. Moreover, the nanorods grown on the hcp seeds are larger in diameter.

Those differences can be attributed to the periodic arrangement and nearest-neighbor distances of the underlying seeds. In the honeycomblike seed pattern, the direction of the nearest neighbor [direction 1, marked as solid arrow in Fig. 1(c) and shown in the inset of the same figure as solid arrow] is the direction that points from the center to the sides of the triangular-shaped nanorod, whereas the pikes of the triangles that form the cross section of the nanorods point in a direction 2 [marked as dotted arrow in Fig. 1(c) and in the inset of Fig. 1(c)] that is rotated 60° in comparison to direction 1. A simple explanation for the triangular-shaped growth is that in direction 1, the distance d_1 between seeds is only ~55% of the distance d_2 between seeds in direction 2 [d_1 and d_2 are shown as white arrows in Fig. 1(c)]. As has been marked out in another publication,[19] for rotationally symmetric nanostructures grown with oblique angle deposition on continuously rotating patterned substrates with distinct seed period d, the saturation radius R_{Sat} of nanorods obeys a power law $R_{\mathrm{Sat}}\sim d^p$, where p is a growth exponent. However, in the experimental part of that work a quadratic template pattern was used, having a higher symmetry than the more complex honeycomb pattern used here. As the distance d_1 between neighbored seeds in direction 1 on the honeycomb pattern is way less than d_2 in direction 2, the growth in direction 1 quickly saturates, resulting in the flat sides of the triangular cross section of the nanorods. In direction 2, the growing nanorod has more space to fill, because $d_2>d_1$. Thus, the "saturation radius" in direction 2 will be greater, leading to the formation of the pikes of the triangular cross section of the nanorod. It has to be marked that the triangular cross section of the nanorods on the honeycomb pattern is not a consequence of the triangular shape of the seeds. Direction 1 of the seeds equals direction 2 of the nanorod pattern after deposition and vice versa, as can be seen in Figs. 1(c) and 2(e): the triangles that form the seeds in the honeycomb pattern are always rotated 60° in comparison to the triangles that form the cross section of the nanorods growing on those seeds, suggesting that the triangular shaped cross section of the Si nanorods should appear on seeds of arbitrary shape as well, as long as the seed template shows a honeycomb arrangement.

The larger diameter of the nanorods grown on hcp seeding spaces can also be explained as a result of the power law mentioned earlier: the larger nearest-neighbor distance [$d=510$ nm (hcp) versus $d=290$ nm (honeycomb) for $D=508$ nm] yields a larger saturation radius and therefore a larger diameter. The circular cross section of those nanorods can be interpreted as a result of the higher symmetry of the hcp pattern compared to the honeycomb pattern: Every surface mound is surrounded by six other seeds in equal distances, yielding a uniform nanorod growth in the plane of the substrate.

Figure 3 shows the diameter distribution $p(w)$ of Si nanorods on honeycomb and hcp patterns for nanosphere diameters of $D=419$ nm and $D=508$ nm. The distributions were determined using statistical analysis of large-scale top view SEM micrographs using SPIP. The term "diameter" describes the following: $w=2\sqrt{A/\pi}$, where A denotes the area of the nanorod cross section detected by SPIP. Therefore, in the case of the honeycomb pattern, w describes the diameter that a nanorod with a circular cross section that has the same area A as the triangular nanorod would have, thus making the $\langle w\rangle$ values of both the hcp and honeycomb pattern comparable.

Honeycomb patterns with $D=419$ nm and $D=508$ nm result in average column diameters $\langle w\rangle=233$ nm and $\langle w\rangle=276$ nm, whereas hcp patterns with the same nanosphere diameters lead to average column diameter values of $\langle w\rangle=316$ nm and $\langle w\rangle=382$ nm. Evidently, a larger nearest-neighbor distance results in nanostructures with larger diam-

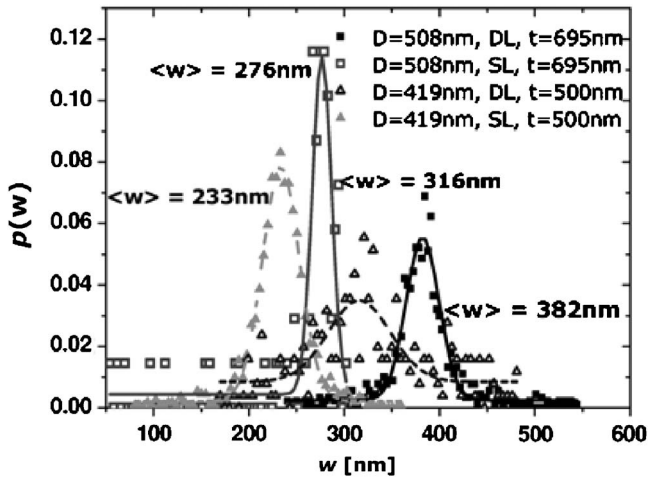

FIG. 3. Diameter distribution of Si nanorods on honeycomb and hcp patterns. $p(w)$ indicates the probability of a rod to have a diameter w. The solid lines ($D=508$ nm) and dotted lines ($D=419$ nm) are Gaussian fits for the data that were used to calculate the average diameter $\langle w\rangle$.

eters. This can be seen when comparing the nanorods grown on honeycomb and hcp patterns of equal nanosphere diameter D, but also when comparing nanorods grown on one type of pattern with different nanosphere diameters D. In good agreement with other publications,[13] the $\langle w\rangle$ values increase nearly proportionally with the inter-rod distances, gaining a fixed $\langle w\rangle/D$ ratio of (0.55 ± 0.01) for the honeycomb pattern and 0.75 for the hcp pattern, suggesting that the density of the nanorod patterns is independent of the pattern size, but varies with the type of pattern. For Ta nanorods grown on honeycomb patterns,[13] a fixed $\langle w\rangle/D$ ratio of (0.39 ± 0.02) was found. The difference to the value for Si nanorods determined in this work leads to the assumption that $\langle w\rangle/D$ is constant if the same growth conditions (namely deposited material, angle of incidence, growth rate, substrate rotational speed) are applied, but might vary due to different geometrical and intrinsic growth conditions (such as different sticking coefficients for Ta and Si, for example).

In Figs. 4(b) and 4(c), 15°-tilted cross-sectional views of Si nanorods deposited on honeycomb and hcp patterns of a height of $h=35$ nm for nanosphere diameters of $D=508$ nm on fused silica are shown, whereas Fig. 4(a) shows nanorods grown on a template-free, bare substrate. Striking differences are clearly observable: the absence of seeds for the impinging particles in the template-free case results in nanorods grown tightly together with diameters that hardly exceed 100 nm. On the contrary, the introduction of hcp and honeycomb template patterns results in a nanorod distribution that replicates the underlying template, with rods having larger diameters as discussed above.

Comparing the micrographs of Figs. 5(a)–5(c), it is observable that the onset height b of the nanostructure growth on the honeycomb patterned seeds shifts from $b=0$ nm for $h=35$ nm (the nanorod covers the whole seed) to $b=(65\pm10)$ nm for $h=95$ nm and finally to $b=(90\pm10)$ nm for $h=150$ nm. An explanation for this development is found with a simple geometrical relation,[20] see Fig. 4(d): Let the distance between adjacent seeds be d. Under a given angle of incidence β (measured to the substrate normal), there exists a certain shadowing length $l=h/\tan(90°-\beta)$, as seeds of height h act as obstacles to the incoming particle flux. In cases where $d<l$, atoms that follow straight line trajectories will impinge not at the bottom of a seed of certain height h, but, due to the shadowing effect of the neighbored seed, at a height h_1 that can be calculated as follows: $h_1=h^*(l-d)/l$. When surface diffusion effects are negligible, characteristic lengths of adatom motion will be small and the particles will not move long distances away from where they attached to the sidewall of the seed. Here, on a honeycomb pattern realized with nanospheres of diameter $D=508$ nm, the nearest-neighbor distance of the adjacent seeds is $d\approx290$ nm. Therefore, for $h=35$ nm, the shadowing length is $l=285$ nm, and $h_1=0$ nm. Thus, the seed gathers particle flux over its whole length, resulting in uniformly shaped nanorods, see Fig. 5(a). Increasing h to 90 and 150 nm leads to h_1 values of 58 and 114 nm, respectively. As can be seen in Figs. 5(b) and 5(c), observable growth starts at $b=(65\pm10)$ nm and $b=(90\pm10)$ nm, respectively. Both values are close to the calculated h_1 data. Hence, surface diffusion effects seem to play a minor role in

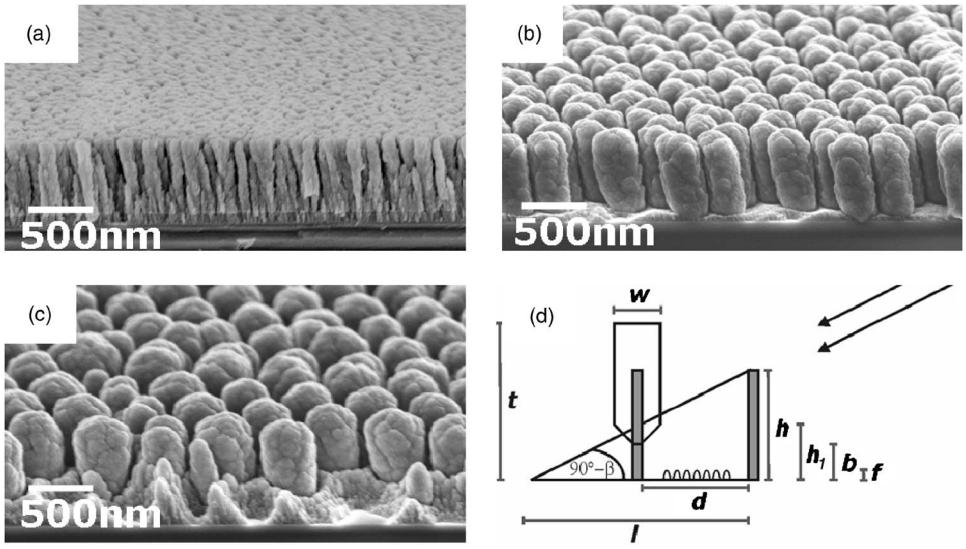

FIG. 4. (a)–(c) 15°-tilted cross-sectional SEM micrographs of Si nanocolumns: (a) without template pattern, (b) honeycomb pattern, $h=35$ nm, and (c) hcp pattern, $h=35$ nm. (d) illustrates the parameters used, where d is the interseed distance, h is the height of the seed, h_1 is the height at which the incoming vapor flux should strike the column for an incoming angle of $90°-\beta$, b is the height of (observable) starting structure growth, f is the height of interseed grown nanostructures, t is the overall height of the nanorod grown on the seed, w is the diameter of the nanorod, and l is the shadowing length.

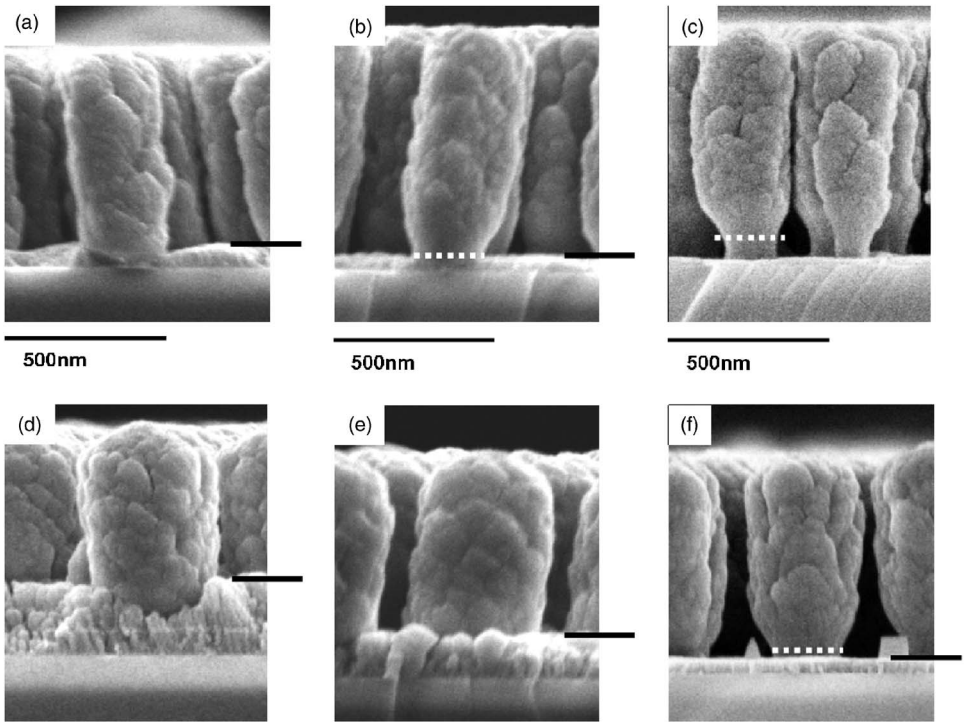

FIG. 5. Cross-sectional SEM micrographs showing Si nanorods on honeycomb patterns [(a)–(c)] and on hcp patterns [(d)–(f)]. Scale is 500 nm for all micrographs. $h=35$ nm for (a) and (d), 95 nm for (b) and (e), and 150 nm for (c) and (f). Solid line: height f of interseed grown nanostructures. Dotted line: height b of onsetting structure growth.

this room temperature GLAD process, whereas geometrical shadowing effects govern the growth mechanism. The deviations between the h_1 and b values might be a result of nondirectional vapor flux. The angular divergence $\Delta\beta$ is a function of the opening of the slit aperture and measures approximately 5°, allowing a minimum angle $\beta=78°$ for Si atoms that are able to reach the substrate. The fact that the surfaces of the columns are rough, showing leaflike substructures and intracolumnar voids, is also an evidence for the ruling influence of the shadowing mechanism compared to surface diffusion effects that would tend to smoothen the GLAD-grown nanorods.

As can also be seen in Figs. 5(a)–5(c), the height f of nanostructures that grow between the seeds decreases from $f=(70\pm10)$ nm for $h=35$ nm to $f=(50\pm10)$ nm for $h=95$ nm, until finally, the interseed-growth disappears for $h=150$ nm. This can be attributed to the increase of the shadowing length l with increasing seed height h as well. Again, the appearance of nanostructures between the seed spaces for cases of $l>d$ [see, for example, Fig. 5(b)] is a result of nondirectional flux that reaches the substrate. As can be seen in Fig. 5(c), if $l\gg d$, all the flux gets caught by the seeds, leaving no interseed growth on the substrate.

Furthermore, it has to be pointed out that the overall nanorod height t is not constant, but increases with increasing seed height. For $h=35$ nm, the rod starts to grow from the bottom of the seed ($b=0$ nm), thus the height of the nanorods is $t=685$ nm and equals the height t_{bare} of the nanocolumns grown on template-free, bare substrates. As discussed earlier, increasing h will result in an increase of h_1 and b. Therefore, the overall height of the nanorods should be increased as well according to $t\approx t_{\text{bare}}+b$. As observed from the SEM micrographs in Figs. 5(b) and 5(c), the heights of the nanorods grown on the seed with $h=95$ nm and $h=150$ nm are both $t=(740\pm30)$ nm. These t values do not exactly fulfill the predicted sum but at least follow the trend of an increase in overall structure height with increasing seed height.

Figures 5(d)–5(f) show cross-sectional SEM micrographs of Si nanorods grown on hcp templates of different seed height h for nanosphere diameters of $D=508$ nm on fused silica. The trends concerning h_1, b, f, and t for those nanostructures are the same as for the nanorods grown on the honeycomb patterned substrate. All observed values for both honeycomb and hcp patterns are listed in Table I. It has to be marked out that there is more interseed growth on the samples with the hcp pattern. This is due to the larger nearest-neighbor distance on the hcp patterns as compared to the honeycomb patterns for the same nanosphere diameter D, yielding a less effective shadowing of the interseed spaces. As the bottom-near region of the Si nanorods was covered by

TABLE I. Shadowing length l, nearest-neighbor seed distance d, particle impinging height h_1, overall nanorod height t, height of starting nanorod growth b, and height of interseed grown nanostructures f as function of seed height h (all in nanometers). The nanosphere diameter measured $D=509$ nm; $d=290$ nm indicates the honeycomb pattern and $d=510$ nm indicates the hcp pattern. For $h=35$ nm and $h=95$ nm, b is not observable for the hcp pattern.

h	l	d	h_1	t	b	f
35	285	290	⋯	685 ± 20	⋯	70 ± 10
		510	⋯	685 ± 20	⋯	235 ± 20
95	773	290	58	740 ± 40	65 ± 10	50 ± 10
		510	32	740 ± 40	⋯	140 ± 20
150	1220	290	114	740 ± 40	90 ± 10	⋯
		510	88	740 ± 40	70 ± 10	60 ± 10

perturbing nanostructures growing between the seeds [see Figs. 5(d) and 5(e)], the value for b could only be observed for $h=150$ nm [see Fig. 5(f)].

IV. CONCLUSIONS

The GLAD growth of Si nanorods on both hcp and honeycomb template patterns by ion beam induced sputter deposition was performed. The patterning of the substrate was done by means of NSL: Au was evaporated through self-assembled mono- and double layers of polystyrene nanospheres. By using the Au dots as etching mask for the silica substrate underneath, the aspect ratio of seed height to interseed distance could be increased up to a factor 5, which resulted in an elongated shadowing length for the successive GLAD experiments and thus to less parasitic growth of Si structures between the seeds. The GLAD experiments were done on templates with different interseed distances and different seed heights. It was found that both cross section and diameter of the nanorods depend on the template type: on honeycomb templates, the nanorods grow triangular-shaped, which could be discussed in terms of different interseed distances in different growth directions. The circular cross section of nanorods grown on hcp patterns is believed to be a result of the higher symmetry of this pattern. As was also pointed out in other publications,[12] there exists a fixed ratio of mean diameter $\langle w \rangle$ to nanosphere diameter D, which was found to be $\langle w \rangle / D = (0.55 \pm 0.01)$ for the honeycomb pattern and 0.75 for the hcp pattern. Besides, it was found that the growth of the Si nanorods on the seeds starts at different heights b for different seed heights h, which in turn resulted in longer nanorods on template patterns with elongated seed heights. This behavior could be explained by adopting a simple geometrical model and under the assumption that the geometrical shadowing effects exceed material-dependent effects, such as surface diffusion, in the used room temperature GLAD regime.

ACKNOWLEDGMENTS

We would like to acknowledge R. Fechner for performing the reactive ion beam etching process.

This work is supported by the project P3 within the DFG research group FOR 522 "Architecture of nano- and microdimensional structure elements."

[1] K. Robbie, L. J. Friedrich, S. K. Dew, T. Smy, and M. J. Brett, J. Vac. Sci. Technol. A **13**, 1032 (1995).
[2] C. M. Zhou and D. Gall, Thin Solid Films **515**, 1223 (2006).
[3] C. Patzig, B. Rauschenbach, W. Erfurth, and A. Milenin, J. Vac. Sci. Technol. B **25**, 833 (2007).
[4] S. R. Kennedy, M. J. Brett, O. Toader, and S. John, Nano Lett. **2**, 59 (2002).
[5] Q. H. Wu, L. de Silva, M. Arnold, I. J. Hodgkinson, and E. Takeuchi, J. Appl. Phys. **95**, 402 (2004).
[6] J. J. Steele, A. C. van Popta, M. M. Hawkeye, J. C. Sit, and M. J. Brett, Sens. Actuators B **120**, 213 (2006).
[7] K. D. Harris, D. Vick, E. J. Gonzales, T. Smy, K. Robbie, and M. J. Brett, Surf. Coat. Technol. **138**, 185 (2001).
[8] T. J. Yim, D. Y. Kim, S. S. Karajanagi, T. M. Lu, R. Kane, and J. S. Dordick, J. Nanosci. Nanotechnol. **3**, 479 (2003).
[9] T. Karabacak, J. P. Singh, Y. P. Zhao, G. C. Wang, and T. M. Lu, Phys. Rev. B **68**, 125408 (2003).
[10] E. Schubert, T. Höche, F. Frost, and B. Rauschenbach, Appl. Phys. A: Mater. Sci. Process. **81**, 481 (2005).
[11] C. M. Zhou and D. Gall, J. Vac. Sci. Technol. A **25**, 312 (2007).
[12] C. M. Zhou and D. Gall, Appl. Phys. Lett. **88**, 203117 (2006).
[13] C. M. Zhou and D. Gall, Appl. Phys. Lett. **90**, 093103 (2007).
[14] B. Fuhrmann, H. S. Leipner, H. R. Höche, L. Schubert, P. Werner, and U. Gösele, Nano Lett. **5**, 2524 (2005).
[15] E. Schubert, J. Fahlteich, T. Höche, G. Wagner, and B. Rauschenbach, Nucl. Instrum. Methods Phys. Res. B **244**, 40 (2006).
[16] E. Schubert, J. Fahlteich, B. Rauschenbach, M. Schubert, M. Lorenz, M. Grundmann, and G. Wagner, J. Appl. Phys. **100**, 016107 (2006).
[17] Image Metrology, www.imagemet.com.
[18] C. Buzea, G. Beydaghyan, C. Elliott, and K. Robbie, Nanotechnology **16**, 1986 (2005).
[19] E. Main, T. Karabacak, and T. M. Lu, J. Appl. Phys. **95**, 4346 (2004).
[20] M. W. Horn, M. D. Pickett, R. Messier, and A. Lakhtakia, Nanotechnology **15**, 303 (2004).